PAPER

A bio-hybrid odor-guided autonomous palm-sized air vehicle

Bioinspiration & Biomimetics

PAPER

A bio-hybrid odor-guided autonomous palm-sized air vehicle

RECEIVED
30 June 2020

REVISED
8 September 2020

ACCEPTED FOR PUBLICATION
1 October 2020

PUBLISHED
16 December 2020

Melanie J Anderson[1], Joseph G Sullivan[2], Timothy K Horiuchi[3], Sawyer B Fuller[1,4] and Thomas L Daniel[1,5,*]

[1] University of Washington, Department of Mechanical Engineering, Seattle WA-98195, United States of America
[2] University of Washington, Department of Electrical and Computer Engineering, Seattle WA-98195, United States of America
[3] University of Maryland, Department of Electrical and Computer Engineering, College Park MD-20742, United States of America
[4] University of Washington, Paul G. Allen School of Computer Science, Seattle WA-98195, United States of America
[5] University of Washington, Department of Biology, Seattle WA-98195, United States of America
[*] Author to whom any correspondence should be addressed.

E-mail: melaniea@uw.edu, jgs6156@uw.edu, timmer@isr.umd.edu, minster@uw.edu and danielt@uw.edu

Keywords: biohybrid, flight, bioinspired, robot, chemical sensing

Supplementary material for this article is available online

Abstract

Biohybrid systems integrate living materials with synthetic devices, exploiting their respective advantages to solve challenging engineering problems. One challenge of critical importance to society is detecting and localizing airborne volatile chemicals. Many flying animals depend their ability to detect and locate the source of aerial chemical plumes for finding mates and food sources. A robot with comparable capability could reduce human hazard and drastically improve performance on tasks such as locating disaster survivors, hazardous gas leaks, incipient fires, or explosives. Three advances are needed before they can rival their biological counterparts: (1) a chemical sensor with a much faster response time that nevertheless satisfies the size, weight, and power constraints of flight, (2) a design, sensor suite, and control system that allows it to move toward the source of a plume fully autonomously while navigating obstacles, and (3) the ability to detect the plume with high specificity and sensitivity among the assortment of chemicals that invariably exist in the air. Here we address the first two, introducing a human-safe palm-sized air vehicle equipped with the odor-sensing antenna of an insect, the first odor-sensing biohybrid robot system to fly. Using this sensor along with a suite of additional navigational sensors, as well as passive wind fins, our robot orients upwind and navigates autonomously toward the source of airborne plumes. Our robot is the first flying biohybrid system to successfully perform odor localization in a confined space, and it is able to do so while detecting and avoiding obstacles in its flight path. We show that insect antennae respond more quickly than metal oxide gas sensors, enabling odor localization at an improved speed over previous flying robots. By using the insect antennae, we anticipate a feasible path toward improved chemical specificity and sensitivity by leveraging recent advances in gene editing.

1. Introduction

Enabled by revolutionary advances in genetic engineering, artificial intelligence, and ubiquitous computing, there has been an explosion of research integrating living and synthetic systems. From robotic prostheses for amputees [1], to implantable deep brain stimulation chips [2], to reprogrammed cellular organisms [3], such biohybrid technologies have yielded breakthroughs in problems at the intersection of biology and engineering. In addition to the deployment of devices into living systems, the complimentary arrangement of integrated living structures into robotic devices—biohybrid robotics—is an emerging technology. Examples of this include utilizing biological cells and tissues as living actuators in artificial machines [4], or creating a biohybrid robot from a living system, such as a jellyfish, by embedding control electronics [5]. In Biohybrid Robotics, living systems are exploited to exceed what is possible in strictly man-made systems.

1.1. Odor localization

Robotic odor localization in natural and artificial

environments is an open challenge of critical importance in life-saving applications. A robot with appropriate chemical sensing capabilities could be used to locate trapped survivors in a disaster, to search for leaks of hazardous chemicals in industrial settings, or to locate explosives or chemical warfare agents in conflict zones. These tasks are well suited to robots because they pose substantial risk to humans or canines. In addition, odor localizing robots could reduce the work of first responders in a disaster by allowing fewer people to search larger areas for survivors. Despite ample research interest and motivation for odor localizing robots, the limited odor sensing performance and stringent size, weight, and power (SWaP) constraints of small robots have hampered their widespread use for such applications.

In contrast, chemical sensing is a universal capability of living organisms across all scales and taxa. Most animals depend on this ability for their survival. Combined with a suitable search strategy, animals can use chemosensing to find the source of chemical emissions which may come from potential mates or food sources [6]. Moreover, flying animals have evolved sophisticated sensing capabilities and olfactory search behaviors that allow them to efficiently search in highly complex 3D environments such as the forest canopy, which include myriad obstacles and turbulent flow. For example, male moths can track females over great distances, detecting female pheromones at concentrations far less than parts per trillion [7]. Female mosquitos use a sense of carbon dioxide to find food [8], and fruit flies sense ethanol [9].

A distinguishing characteristic of plume tracking by animals is the use of near-instantaneous information present in the plume [6, 10]. Plumes in the air typically consists of a patchy distribution of filaments containing high chemical concentration interspersed among large areas of low concentration. This is because convection dominates over diffusion for transport in atmospheric flow, which is turbulent [6].

1.2. Flying smelling robots

Recent research has strived to approach the remarkable odor search capability of living systems using robots. Flying robots are well suited to this task as they can search for odor sources at various altitudes, avoid difficult terrain, and manage obstacles without sophisticated ambulatory systems. Important advances in plume source localization with flying robots include a 1 m multi-rotor drone that follows an outdoor methane plume to its source in two-dimensional space [11]. This drone used semiconductor metal oxide (MOX) sensors, which have low chemical specificity, a slow rise time and long recovery period in the presence of high gas concentrations [12, 13]. To achieve reliable readings, the drone must pause at each sampling location for 20 s for the sensor to stabilize, necessitating a search time lasting tens of minutes, nearly as long as the drone's battery life. In another recent work, Luo *et al* [14] showed that with improved signal processing, an array of MOX sensors could extract odor information from a plume on a short timescale. However, their signal processing algorithm is computationally intensive, and requires constant communication to an offboard computer with a powerful GPU. Burgués *et al* [15] has achieved odor localization in a multi-room space using a calibrated MOX to sense an indoor chemical source on a palm-sized drone. They were able to consistently locate odor sources, but their approach relied an external absolute positioning system, a map of the room, and repeated traverses, which are not typically available in environments of practical interest. Shigaki *et al* implement a moth-inspired strategy on a pocket-sized drone using MOX sensors [13]. They apply an inverse sensor model in order to improve the signal from the MOX sensors and are able to successfully fly toward an alcohol source over a 2 m distance. Other work on source localization has investigated different sources such as light which allows a gradient search unaffected by wind. One example of this shows that a small drone platform carrying a light sensor can use a deep reinforcement learning policy to find the source of a light even in the presence of obstacles [16]. Hence the state of the art continues to be challenged by the speed and reliability of suitably small synthetic chemical sensors and size-constrained navigation systems.

1.3. Electroantennograms (EAGs) and natural chemical sensing

Biological odor detectors, such as moth antennae, outperform state-of-the-art (engineered) portable chemical sensors in detection speed, sensitivity, and chemical selectivity. The extreme sensitivity and rapid response times of natural chemical sensing arises, in part, from an energy dependent G protein-coupled amplification system that can convert single molecule detections into electrical signals in odor-detecting neurons of the moth antennae [17]. These electrical signals, known as EAG, can be measured using highly sensitive amplifiers. While moths discriminate between odors by sensing signals from individual neurons, EAGs are the combined response of all the neurons.

Use of EAGs coupled to the antennae of moths has been previously demonstrated on mobile robots for chemical plume tracking. Notable examples of biohybrid robotic systems using living sensors on ground robots include a mobile robot in a wind tunnel using a moth EAG [18], an odor tracking mobile robot steered based on input from a moths' ambulation motions on a sensitive trackball [19], and a ground robot capable of avoiding collisions by using a fly's visual system to perform optic flow estimates [20]. There have also been some systems integrating biological and bioinspired components on flying systems such as a drone being steered by an off-board moth on

a trackball [21] and the development of an algorithm to improve an EAG signal onboard a tethered 0.5 m drone [22].

1.4. The 'Smellicopter': a biohybrid system

In this work, we introduce the use of an insect's chemosensory apparatus on a flying robot dubbed the 'Smellicopter'. By doing so, we leverage the sophisticated and fast G-protein-mediated chemosensing capabilities that have evolved in biology to provide a sensor with a speed that better matches rapid motions possible with flight. Our EAG-based system uses antennae from the hawkmoth *M. sexta* for a lightweight (1.5 g) and extremely low-power (2.7 mW) sensor. We show that it has a much faster response than MOX sensors, and deploy it on a small, palm-sized 30 g hovering four-rotor aircraft. We then equipped this biohybrid system with a sensor suite that allowed it to control its position and avoid obstacles while moving through confined spaces fully autonomously. To enable the robot to navigate a chemical plume, we additionally introduced wind fins fixed to the robot, which cause it to passively orient into the wind. This allows for a simple, reactive search that relies on the robot operating in a coordinate system rotated to a wind-oriented reference frame at all times. In previous work [23], we presented a proof of concept for this system. Here, we expanded its capabilities to include operation in confined spaces with obstacles and provide a more detailed analysis of EAG and robot system performance. We show that our biohybrid robot navigates to the source of an airborne odor plume in a confined wind tunnel repeatedly over 15 independent trials, and uses laser ranged distance estimates to avoid obstacles. Our robot uses a bio-inspired cast-and-surge strategy, without any need for external position information such as from the global positioning system (GPS).

The aggregation of these advances represents a significant advance in robotic plume source localization because with them we are able to, for the first time, quickly and fully autonomously, navigate to a chemical plume source in an environment including obstacles as would be encountered in many real-world applications. Furthermore, we anticipate that our biological sensor has the potential for designing chemical specificity using recent advances in genetic engineering to express chemical-specific chemosensors [24].

2. Design and system architecture

2.1. Structure and control architecture

Our palm-sized air vehicle, the smellicopter (figure 1(a)), is built from a commercially available quadcopter, the Crazyflie 2.0 (Bitcraze AB). We use two additional commercial sensor decks that have functions critical for autonomy: the flow deck (Bitcraze AB) which has down-facing optical-flow and range sensors and the multi-ranger deck (Bitcraze AB) which has five-directional range sensing. The optical-flow sensor provides body-frame velocity measurements that allow the quadcopter to hover in-place indoors without GPS or a motion capture camera system. The laser range sensors provide range measurements in four directions in the horizontal plane (forward, back, left, right), allowing the quadcopter to detect and navigate around obstacles. In addition to the commercial components, we have added two custom innovations: our antennal neural signal amplifier deck (ANSAD) (figure 1(b)) and the aerodynamic fins. The ANSAD generates an EAG providing the Smellicopter with odor information. The aerodynamic fins passively steer the platform upwind to perform the odor localization algorithm. The component configuration is shown in figure 1(c).

The Crazyflie, built from extensible open-hardware, occupies just 85 cm^2 and weighs only 23 g, placing it among the smallest autonomous air vehicles on the market and making it ideal for indoor use. When carrying the additional components, the Crazyflie can fly for up to 7 min from a single cell lithium–polymer battery with 250 mAh of capacity.

Our platform communicates over a 1 Mbyte/s bluetooth radio link, receiving EAG data, range information, and state information from the Crazyflie, which is provided to a navigation program (figure 1(d)). This program then uses the radio to send velocity commands back to the Crazyflie. Like Luo *et al* [14], we used an external computer to run the simple navigation program. However, our program has minimal computational requirements and can be fully implemented within the 32 bit microcontroller on the Crazyflie. In this work we use an external computer solely to simplify the workflow of implementing and testing the navigation program.

2.2. On-board EAGs and MOX sensors

Antennae serve as critical sensory organs for insects and other arthropods. In addition to their capacity to sense wind [25] and vibrations [26], antennae most notably provide olfactory information to the insect to find food and mates [27]. Chemical sensing follows from a complex cascade of molecular interactions [17]. Volatile compounds diffuse into the interior of the antenna where they then bind to odor-binding proteins. Those complexes then bind to, and activate, G-protein receptor molecules on the membranes of chemosensory neurons populating the interior of the antenna. Once activated, G-protein-mediated pathways provide a whole cell response that greatly amplifies the influence of a single odorant molecule. That amplified response yields, in turn, an action potential that propagates down the antennal neuron to the brain of the insect. With thousands of olfactory neurons in an antenna [28], an EAG represents their aggregate electrical activity by the voltage

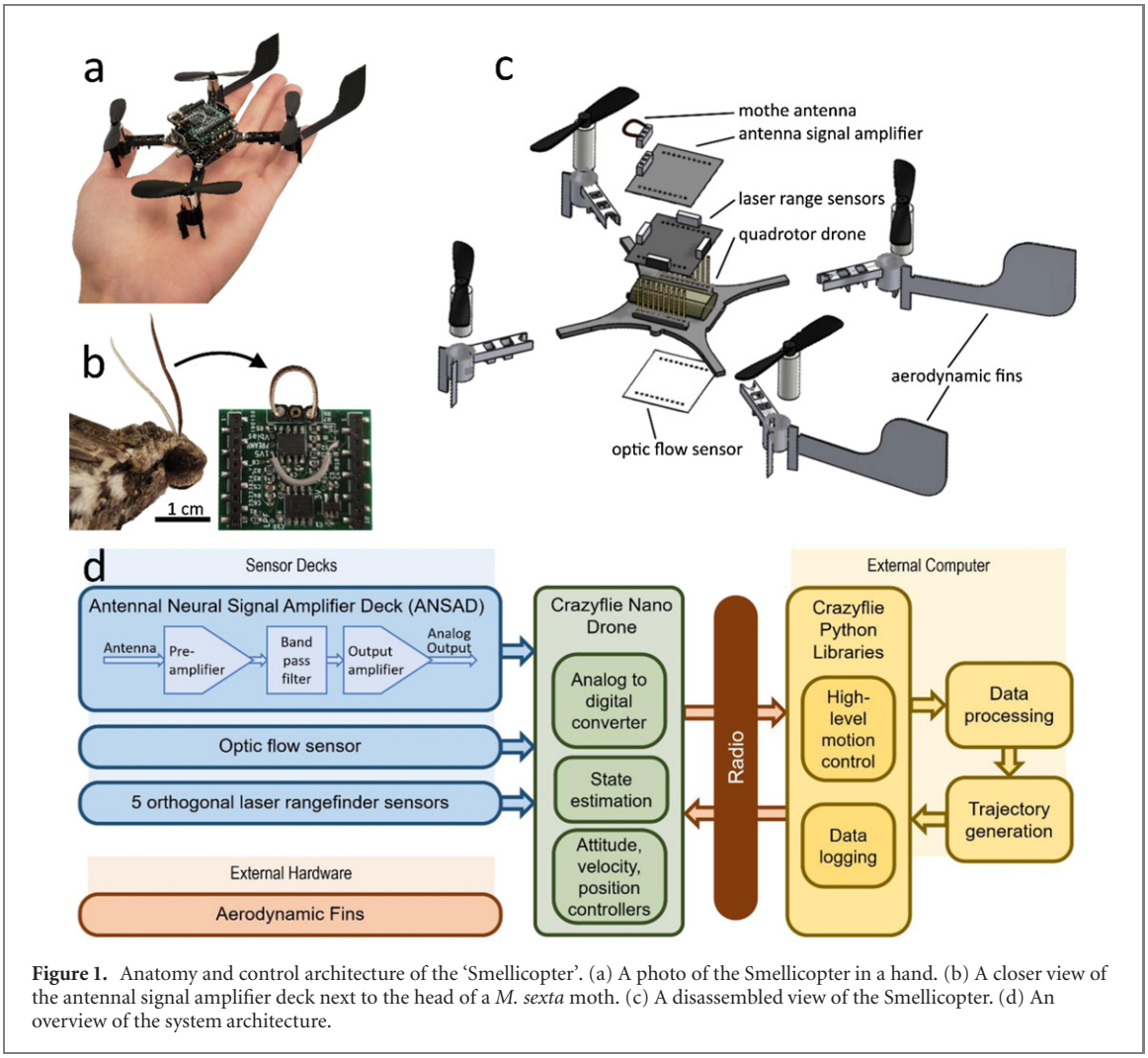

Figure 1. Anatomy and control architecture of the 'Smellicopter'. (a) A photo of the Smellicopter in a hand. (b) A closer view of the antennal signal amplifier deck next to the head of a *M. sexta* moth. (c) A disassembled view of the Smellicopter. (d) An overview of the system architecture.

drop across the length of the antenna. An EAG therefore provides an electrical reading of a neural process, much as is done for electromyograms (EMG) or electroencephalograms (EEG).

The ANSAD circuit, which produces the EAG, consists of three cascaded filtering and amplification stages that are tuned to the responses in antennae from *M. sexta*, resulting in a low-noise, highly amplified EAG signal. The ANSAD weighs 1.5 g and consumes only 2.7 mW, imposing minimal weight and power requirements on the platform [23]. The ANSAD circuit board is designed to mount directly onto the Crazyflie drone platform in the same manner as the other commercial add-on decks. The antenna is oriented toward the front of the drone, where the flow from the rotors will pull air over the antenna. This downwash is suspected to enhance the signal, much like how flapping wings can enhance the flow of air over the antenna of a flying insect, thereby increasing the amount of air which can be sampled for odors [29].

Antennae isolated from cold anesthetized *M. sexta* moths were connected to the ANSAD via 75 μm diameter stainless steel electrodes. This preparation results in an EAG that responds to particular volatile chemicals rapidly, with a maximum bandwidth of 10 Hz [12], providing the capability to make multiple chemical detections in quick succession. We tested the EAG sensor by stimulating the antenna with the custom floral mixture presented in [23], comprised of compounds present in the flower *D. wrightii* [30], a common floral nectar source for *M. sexta*. This mixture is an attractant for both female and male moths and is effective in producing EAG responses. These antennae continued to produce signals for at least 2 h and up to 4 h. The signal strength, however, continuously declines over this period as has been noted in other insect species [12]. The lifespan of the severed antenna is still many times the flight time of a drone and can be used for multiple successive trials.

We tested the performance of the ANSAD and compared it to a similarly sized commercial MOX sensor, the MiCS-5524, which consumes approximately 150 mW and is nearly identical to the sensors used in other odor localization work [13, 14]. We deposited 5 μl of the scent mixture and 10 μl of 50% ethanol on a 1 cm diameter filter paper placed inside of a disposable pipette. When the pipette is squeezed it expels a puff of floral and ethanol scented air. The EAG and MOX sensors were placed adjacent to one another

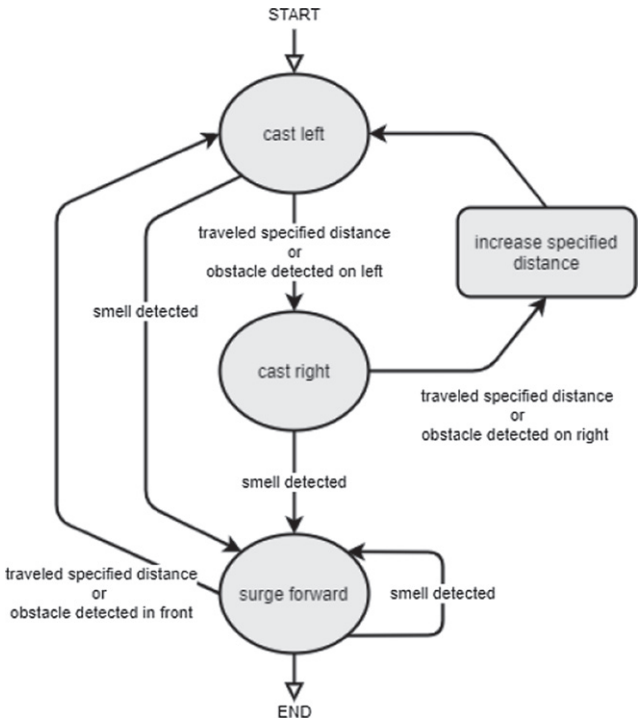

Figure 2. Flow chart of the cast-and-surge algorithm. The algorithm begins with casting left for a specified distance and then casting right for that same distance. For each successive cast left and right, the casting envelope distance is increased. If a smell is detected at any time during this process, the algorithm switches to upwind surging for a specified distance. If another smell is encountered during a surge, the surge will continue. If the Smellicopter has surged for the specified distance and has not encountered another smell, it will switch back to the initial casting left stage and reset the casting distance to the starting amount. Additionally, obstacle avoidance can be added to the strategy. When an obstacle is detected in the direction that the Smellicopter is currently moving, the Smellicopter will jump to the next state in the algorithm. The cast-and-surge algorithm is for finding and following a plume. Source detection is another task which is not yet covered. The algorithm is manually terminated before the Smellicopter collides with the front of the wind tunnel.

inside of an OMEGA mini wind tunnel with airspeed at 2.5 m s^{-1}. The MOX sensor is facing toward to upwind direction and the EAG sensor is placed in the upright position same as if it were mounted on the drone. The pipette is placed perpendicular to the air flow at the intake of the wind tunnel to ensure that the antennal response recorded is due to chemical stimulus and not to mechanical stimulus from the puffed air. The pipette is puffed by hand at various frequencies. Each stimulus results in an obvious spike in the output signal that decays in a fraction of a second. We quantified the rise and fall times by computing the time between 10 percent of the peak value to the time of the peak value and from the time of the peak value to 10 percent of the peak value respectively.

2.3. Cast-and-surge localization with passive fins

The Smellicopter implements an olfactory search using a navigation algorithm that is inspired by the insect foraging in a single horizontal plane [11] (see supplemental video) (https://stacks.iop.org/BB/16/026002/mmedia). Flying odor-tracking insects will often fly in a crosswind casting pattern, and upon encountering an odor, the insect will steer into the wind [27]. This crosswind casting can be in the form of spiraling/looping [12, 13, 31], zigzagging [13, 31, 32], or simple back-and-forth crosswind movement with no upwind component [32]. Although insects perform three-dimensional tracking while following odor plumes, 3D algorithms have not yet been implemented on flying platforms. Luo [14] does locate a source in 3D but uses a multi-stage approach which consists of a separate vertical search algorithm to find the altitude of a turbulent plume and then switching to a horizontal only search algorithm to locate the source. Our implementation (figure 1(d)) uses a crosswind casting strategy, and it requires that the Smellicopter is in an environment with relatively consistent wind or airflow. We chose to focus on deploying a 2D cast-and-surge algorithm (figure 2), which is similar to the existing casting and surging strategies that have been extensively tested in the literature mentioned above.

Crosswind casting demands that the system has wind orientation capabilities. Past efforts to perform olfactory search using autonomous UAVs have used numerical methods to actively estimate the wind vector. Neumann *et al* [11] used the law of cosines to compute the wind vector from the wind triangle, but that approach required an airspeed reference function that was derived from wind tunnel characterization of the drone. Luo *et al* [14] estimated the direction of the wind by filtering the UAV attitude in response to the wind, but this method requires that the wind speed

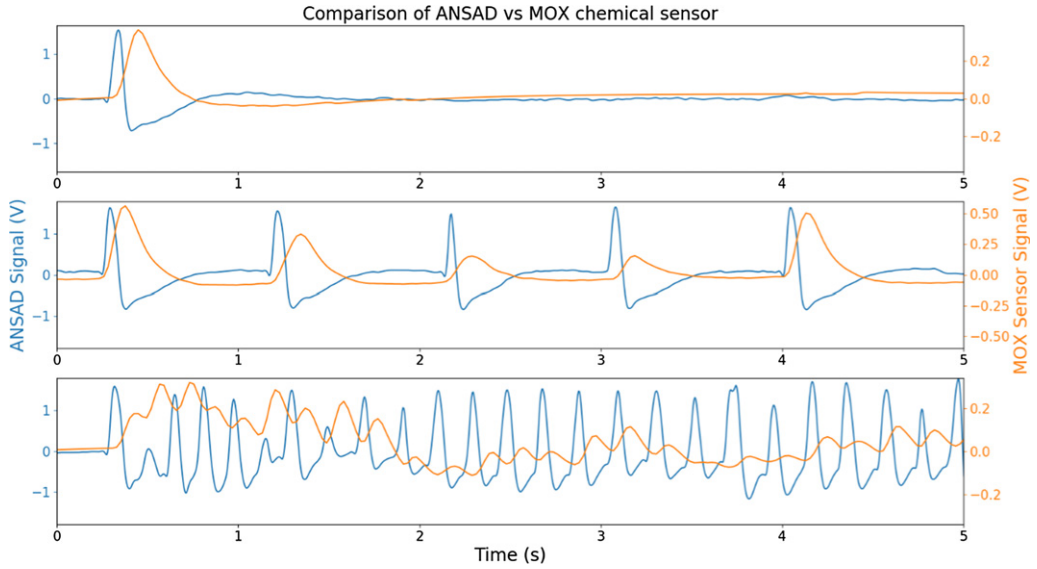

Figure 3. EAGs from a moth antenna and signals from metal oxide sensors. Three trials show the time course of signals recorded from the ANSAD sensor and the MOX sensor when stimulated with scented air. 5 μl of custom floral scent [23] and 10 μl of 50% ethanol is deposited on a 1 cm diameter filter paper disk and placed into a disposable pipette. The stimulus is hand puffed perpendicular to the intake of an OMEGA mini wind tunnel with windspeed at 2.5 m s^{-1}. In (**a**), the stimulus is delivered once. In (**b**) and (**c**), the stimulus was delivered by hand at approximately 1 and 5 Hz with the aid of a metronome. Data were recorded at approximately 42 samples per second.

imparts an attitude bias that exceeds the uncertainty of the attitude state estimate.

In contrast, we have used a passive control scheme to force the Smellicopter to constantly face upwind by adding thin plastic wind vanes to the rear motor mounts and by modifying its yaw controller. The yaw *angle* controller of the Smellicopter is disabled, and the gain of the yaw *rate* controller is reduced, which allows exogenous torque disturbances to perturb the Smellicopter's yaw *angle*. The wind vanes are oriented such that when the Smellicopter is not facing upwind, the force of the wind airflow on the vanes imparts a yaw torque to rotate it into the wind. This process works much like a weathervane. The Smellicopter holds its translational position using the downward-looking optic flow sensor. This method works well in a steady breeze, which could be encountered in situations such as a mine shaft or in a building with opposing windows open.

Volatile chemicals are detected by simple thresholding of the EAG signal using the following method. Prior to the trials, the Smellicopter is manually hovered in and out of the chemical plume and the threshold is manually inputted into the search algorithm. This is necessary because of small variations between antennae. If the EAG signal exceeds this threshold during flight, a surge is triggered. This strategy will bring the insect or robot increasingly closer to an odor source with each surge. Moreover, the casting allows the insect or robot to relocate the plume even if there is a slight shift in the wind direction or movement of the source; however, the algorithm requires that the Smellicopter is facing upwind most of the time.

2.4. Multisensor integration with obstacle avoidance

The Smellicopter is equipped with a *MultiRanger* deck that uses four infrared range sensors that permit obstacle detection and thus allows it to navigate around obstacles while performing an odor localization strategy. The fifth range sensor which gives a distance measurement to obstacles above the Smellicopter is unused. To avoid obstacles, the Smellicopter takes range measurements in four directions, ten times per second. When a range measurement in the direction of the Smellicopter's current heading falls below 20 cm, then the Smellicopter will change direction by advancing to the next state of the cast-and-surge search behavior.

For the odor localization and obstacle avoidance trials, we used a source consisting of a 2 cm filter paper disk with 5 μl of the scent mixture deposited on it. The trials take place in a wind tunnel 2 m long by 1 m wide by 1 m tall with a windspeed of approximately 1 m s^{-1}. The source is placed at the front of the wind tunnel, upwind of the experimental area.

3. Results

3.1. On-board EAGs vs metal oxide sensors

We compared the sensitivity and response of the EAG produced by our sensor to a commercial MOX sensor similar to those used in other odor localization studies [13, 14] (figure 3). Our EAG sensor and a metal oxide (MiCS-5524) sensor were tested simultaneously with floral scent and ethanol. Twice as much stimulus (ethanol) was used for the MOX sensor as was used for the EAG sensor (floral scent) to produce a visible

Table 1. EAG vs MOX comparison. Signal rise time is the time from 10% of peak to peak, signal fall time is the time from peak to 10% of peak.

		Peak height	Rise time	Fall time
EAG	Mean	1.425	0.045	0.045
	Standard deviation	0.098	0.015	0.007
MOX	Mean	0.413	0.104	0.198
	Standard deviation	0.095	0.013	0.021

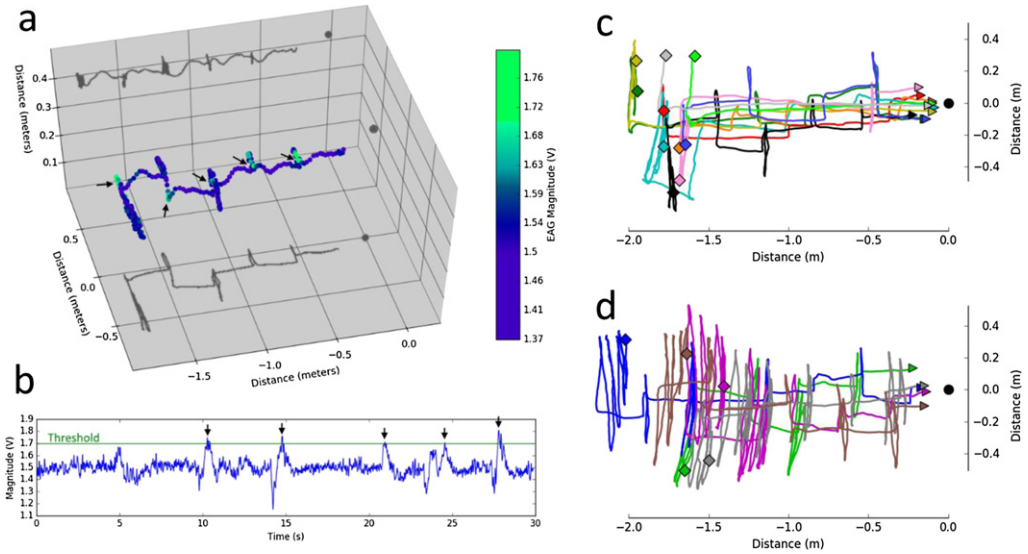

Figure 4. Odor localization trials. (a) A single trial of the Smellicopter navigating to the source of the odor plume. Wind speed was estimated to be approximately 1 m s^{-1}. The multicolored line shows the 3D trajectory of the Smellicopter as estimated from its optic flow-based position estimator. Grey lines show the vertical and horizontal projections of the 3D trajectory and grey circles show the location of the source relative to each path. The color bar indicates the voltage level of the signal from the ANSAD as the trial progresses where blue is no odor sensed, light blue is some odor sensed, and green is enough odor sensed to trigger a surge in the behavior. Places where a surge is triggered are identified with black arrows. The test is performed in a wind tunnel with the wind direction from right to left. The Smellicopter's position is estimated from onboard sensors. (b) The EAG signal of the trial shown in (a). Activity that surpasses the threshold triggers a surge in the search strategy and is marked with a black arrow. (c) and (d) Additional tests in a top-down view. Upper plots are trials with a duration of less than 30 s and lower plots are trials with a duration of greater than 30 s.

signal from the MOX sensor. A digital filter is applied to the MOX sensor signal with the same transfer function as the analog filter in the ANSAD circuit, which has low and high cutoff frequencies at approximately 2 Hz and 60 Hz respectively.

The EAG signal rise time (time from 10% of peak to peak) and fall time (time from peak to 10% of peak) were less than half of that of the MOX signal (table 1). The EAG signal has a negative component due to the filtering circuitry. The sensors were placed directly adjacent to one another in the wind tunnel, but due to the size of the sensors, the separation between the sensing portions was around 1.5 cm. This separation and the patchy nature of airborne odor plumes causes the responses from the sensors vary between stimulations.

3.2. Cast-and-surge localization with passive fins

For our 2D cast-and-surge tests, the Smellicopter took off to a height of 40 cm and then hovered while the yaw control was lowered to allow passive upwind orientation using the aerodynamic fins. It then began left-right crosswind casting with increasing casting amplitude until a volatile chemical was detected via the ANSAD, at which time it surged 25 cm upwind (i.e. forward). In the absence of additional chemical signals, it resumed crosswind casting. The tests were manually terminated once it is approximately 10 cm downwind of the source to avoid the Smellicopter colliding with the intake screen of the wind tunnel. The plots in figure 4 show the Smellicopter's estimate of its position as it flies through the wind tunnel. This estimate is susceptible to drift over time, so each ending distance to the source (table 2) is determined by measuring the distance shown through an overhead camera. In 14 out of 15 trials, the Smellicopter ended within 4 cm of the source in the crosswind direction. All trials ended within 6 cm of the source in the crosswind direction. Distance to the source in the direction parallel to the wind direction is not recorded since the trials are stopped before the Smellicopter collides with the intake screen of the wind tunnel.

3.3. Multisensor integration with obstacle avoidance

To test the obstacle avoidance capability of our plat-

Table 2. Summary data for odor localization trials. For 15 trials we monitored the search duration and path length for the Smellicopter flight in a wind tunnel.

Trial	Starting position x (m)	Starting position y (m)	Ending distance to source (cm)	Time duration (s)	Length of total path (m)
1	−1.95	0.07	−4.0	23.91	4.27
2	−1.65	−0.51	5.5	73.14	8.12
3	−1.78	−0.05	2.0	12.40	2.27
4	−2.02	0.31	0.5	79.63	14.27
5	−1.78	−0.27	−1.0	45.78	5.36
6	−1.41	0.02	−0.5	85.32	15.60
7	−1.96	0.27	−2.0	17.95	3.33
8	−1.50	−0.44	1.0	93.12	16.98
9	−1.68	−0.28	0.5	12.44	2.24
10	−1.72	−0.56	−3.0	29.88	5.28
11	−1.64	0.22	−4.0	100.47	11.33
12	−1.68	−0.48	4.0	22.03	3.86
13	−1.59	0.30	0.0	15.90	2.14
14	−1.65	−0.26	−4.0	28.01	3.11
15	−1.77	0.30	−0.5	11.16	2.07
Mean	−1.72	−0.09	−0.37	43.41	6.68
StDev.	0.17	0.33	2.83	33.07	5.27

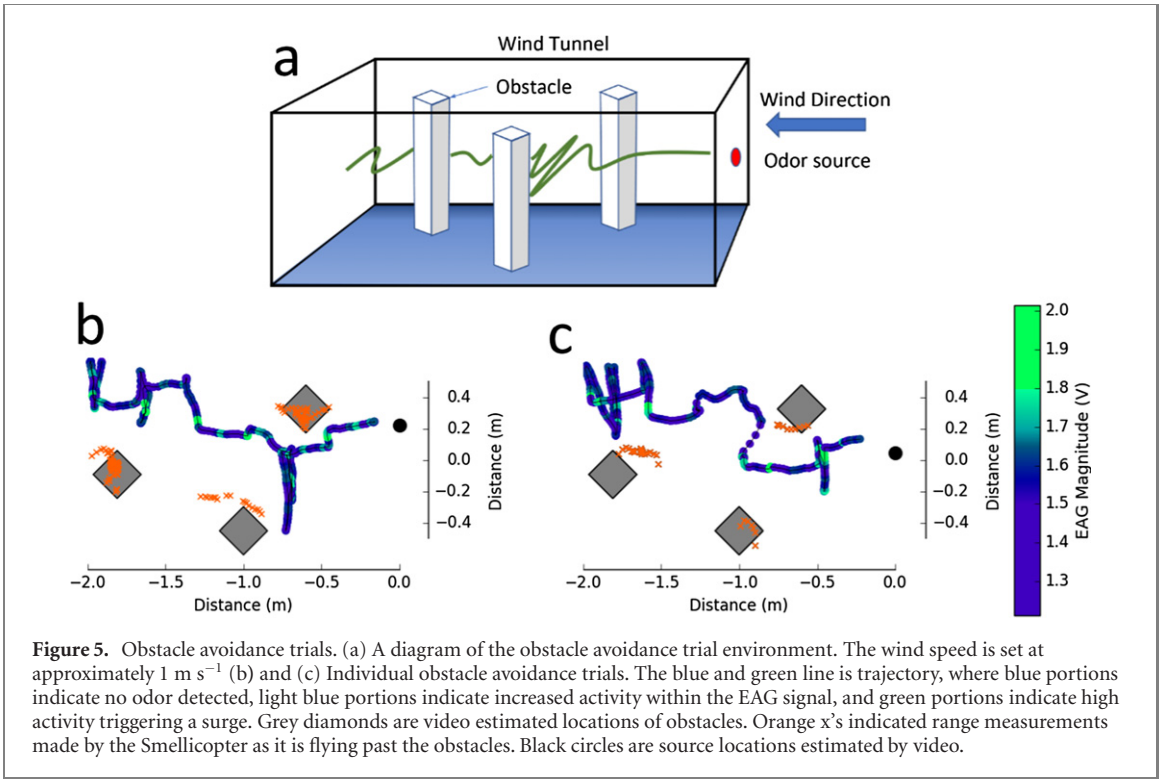

Figure 5. Obstacle avoidance trials. (a) A diagram of the obstacle avoidance trial environment. The wind speed is set at approximately 1 m s^{-1} (b) and (c) Individual obstacle avoidance trials. The blue and green line is trajectory, where blue portions indicate no odor detected, light blue portions indicate increased activity within the EAG signal, and green portions indicate high activity triggering a surge. Grey diamonds are video estimated locations of obstacles. Orange x's indicated range measurements made by the Smellicopter as it is flying past the obstacles. Black circles are source locations estimated by video.

form, we set up cardboard obstacles inside the wind tunnel environment outlined in the previous experiments (figure 5(a)). The wind speed was set to approximately 1 m s^{-1}. As above we used a source consisting of a 2 cm filter paper disk with 5 μl of custom scent mixture deposited on it. Trials were manually terminated when the Smellicopter came within approximately 10 cm of the source in the direction parallel to the wind direction to prevent collision with the front of the wind tunnel. The plots in figure 5 show the Smellicopter's estimate of its position as it flies through the wind tunnel. This estimate is susceptible to drift over time, so the ending positions are determined by measuring the distance shown through an overhead camera. The Smellicopter was able to successfully localize the source of the odor while avoiding the obstacles presented. Figure 5(b) and 5(c) show two successful trials of the Smellicopter performing odor localization as well as obstacle avoidance. In each trial, the Smellicopter navigated through the obstacles and ended within 4 cm of the source in the crosswind direction.

4. Discussion

This study has drawn on the synergy between the engineerability of synthetic robotics and the out-

standing performance of naturally-occurring sensory systems to create a device that combines the best of both worlds. Thus, we developed a biohybrid flight system capable of autonomously localizing a chemical source via a biologically-inspired plume tracking behavior. It provides a novel solution to a challenging technological problem; one with stringent SWaP constraints. Interestingly, the development of bio-hybrid robotic systems has seen dramatic growth over the last decade, with some systems containing microelectronics embedded into intact living systems [33–36], devices that contain sensory structures embedded onto robotic platforms [18, 20, 37], and even robotic platforms with integrated cultured muscle cells as actuators [4]. All these efforts seek to take advantage of the sensor or actuator efficiency of living systems along with the fabrication advantages of artificial systems.

While the integration of natural and synthetic systems presents exciting new horizons for autonomous aerial vehicles, operating under stringent SWaP constraints poses both challenges and opportunities. Indeed, our motivation to turn to natural sensory structures was largely motivated by these constraints. Using the living antennae of moths with electronic amplifiers to generate EAGs is a weight and power efficient way to acquire chemical information, but antennae have a finite lifetime, thus limiting their long-term deployment. That said, the battery life of the Crazyflie is significantly shorter than the longevity of antennae providing EAGs. Typical flight times are constrained to be less than about 10 min for the Crazyflie and our associated additional hardware. In contrast, we were able to maintain stable EAGs for more than 2 h and up to 4 h. Additionally, explanted antennae can be stored on ice for several days prior to deployment on the Smellicopter, suggesting a viable strategy for deployment in locations remote from a laboratory.

Insect antennae respond to hundreds of volatiles [28, 38–40], providing both a challenge and an opportunity. The insect is able to identify particular chemicals or mixtures by differentiating between the neurons, but out current configuration measures the aggregate electrical activity of the neurons by the voltage drop across the length of the antenna. Our current configuration can function well with any number of volatile cures, but specific responses to a single odorant is challenging if multiple volatiles are present in the plume. Emerging CRISPR technologies, however, may allow gene editing of antennae to target specific volatiles [24]. Future efforts can focus on multiple antennae, each designed for a specific volatile, thus providing detection of more complex chemical signals.

Other limitations related to SWaP constraints include our method for collision avoidance. The current configuration using four side-facing laser range sensors is a lightweight solution to avoid collisions, but works poorly under conditions where the sensor view is tangential to the object or the object is small enough to fit between the detection beams. This limitation could be addressed by adding a sweeping yaw motion to the search algorithm, but this movement is currently challenging due to our passive upwind orientation. Collision avoidance could also be improved by adding ultra-miniature camera systems, but this would require significant processing for detecting close objects against a visual background and estimating their distance, an approach that could easily exceed the available computational or power resources for small autonomous air vehicles.

Despite these limitations, our biohybrid system holds promise for many applications in which we have used other odor localization solutions, notably the myriad situations in which used dogs have been used to detect and locate drugs, missing people, or volatiles from explosives. Moreover, this aerial robotic system can provide a valuable platform on which we can experimentally explore the complex 3D interaction between aerial propulsion, odor localization strategies, and airflow in the environment.

Supplemental information

Video of Smellicopter in a wind tunnel with and without obstacles.

Author contributions

MA contributed to the conception and design of the work, creation of the software and hardware, data acquisition and analysis, and drafting and revision of the manuscript. JS contributed to the design of the work, creation of the software and hardware, and drafting and revision of the manuscript. TH contributed to the conception of the wind fins and drafting and revision of the manuscript. SF contributed to the conception of the work and drafting and revision of the manuscript. TD contributed to the conception of the work and drafting and revision of the manuscript.

Competing interests statement

The authors declare no competing interests.

Acknowledgments

This work has been supported by the National Defense Science and Engineering Graduate Fellowship, the Washington Research Foundation, the Joan and Richard Komen Endowed Chair, and the Air Force Office of Scientific Research (AFOSR), Grant Nos. FA9550-14-1-0398. We wish to thank Drs. Jennifer Talley, Kevin Brink, Jeffrey Riffell and Mark Willis for suggestions and advice throughout the preparation of this work. Matthew Mann and Amanuel Mamo both assisted with data collection.

ORCID iDs

Melanie J Anderson https://orcid.org/0000-0001-8555-6857

References

[1] Herr H M and Grabowski A M 2011 Bionic ankle-foot prosthesis normalizes walking gait for persons with leg amputation *Proc. R. Soc. B.* **279** 457–64

[2] Heeron J, Denison T and Chizeck H J 2015 Closed-loop DBS with movement intention *7th Int. IEEE/EMBS Conf. on Neural Engineering* 844–7

[3] Gander M W, Vrana J D, Voje W E, Carothers J M and Klavins E 2017 Digital logic circuits in yeast with CRISPR-dCas9 NOR gates *Nat. Commun.* **8** 15459

[4] Ricotti L *et al* 2017 Biohybrid actuators for robotics: a review of devices actuated by living cells *Sci. Robot.* **2** eaaq0495

[5] Xu N W and Dabiri J O 2020 Low-power microelectronics embedded in live jellyfish enhance propulsion *Sci. Adv.* **6** eaaz3194

[6] Riffell J A, Abrell L and Hildebrand J G 2008 Physical processes and real-time chemical measurement of the insect olfactory environment *J. Chem. Ecol.* **34** 837–53

[7] Anton S and Hansson B 1995 Sex pheromone and plant-associated odour processing in antennal lobe interneurons of male *S. littoralis* (*Lepidoptera: Noctuidae*) *J. Comp. Physiol.* A **176** 773–89

[8] Lahondère C, Vinauger C, Okubo R P, Wolff G H, Chan J K, Akbari O S and Riffell J A 2020 The olfactory basis of orchid pollination by mosquitoes *Proc. Natl Acad. Sci. USA* **117** 708–16

[9] Budick S A and Dickinson M H 2006 Free-flight responses of Drosophila melanogaster to attractive odors *J. Exp. Biol.* **209** 3001–17

[10] Mafra-Neto A and Cardé R T 1994 Fine-scale structure of pheromone plumes modulates upwind orientation of flying moths *Nature* **369** 142–4

[11] Neumann P P, Hernandez Bennetts V, Lilienthal A J, Bartholmai M and Schiller J H 2013 Gas source localization with a micro-drone using bio-inspired and particle filter-based algorithms *Adv. Robot.* **27** 725–38

[12] Martinez D, Arhidi L, Demondion E, Masson J B and Lucas P 2014 Using insect electroantennogram sensors on autonomous robots for olfactory searches *J. Vis. Exp.* **90** e51704

[13] Shigaki S, Fikri M and Kurabayashi D 2018 Design and experimental evaluation of an odor sensing method for a pocket-sized quadcopter *Sensors* **18** 3720

[14] Luo B, Meng Q, Wang J and Zeng M 2018 A flying odor compass to autonomously locate the gas source *IEEE Trans. Instrum. Meas.* **67** 137–49

[15] Burgués J, Hernández V, Lilienthal A and Marco S 2019 Smelling nano aerial vehicle for gas source localization and mapping *Sensors* **19** 478

[16] Duisterhof B P, Krishnan S, Cruz J J, Banbury C R, Fu W, Faust A, de Croon G C H E and Reddi V J 2020 Learning to seek: deep reinforcement learning for phototaxis of a nano drone in an obstacle field (arXiv:1909.11236)

[17] Spehr M and Munger S D 2009 Olfactory receptors: G protein-coupled receptors and beyond *J. Neurochem.* **109** 1570–83

[18] Kuwana Y, Nagasawa S, Shimoyama I and Kanzaki R 1999 Synthesis of the pheromone-oriented behaviour of silkworm moths by a mobile robot with moth antennae as pheromone sensors *Biosen. Bioelectron.* **14** 195–202

[19] Ando N and Kanzaki R 2017 Using insects to drive mobile robots—hybrid robots bridge the gap between biological and artificial systems *Arthropod Struct. Dev.* **46** 723–35

[20] Huang J V, Wei Y and Krapp H G 2019 A biohybrid fly-robot interface system that performs active collision avoidance *Bioinsp. Biomim.* **14** 6

[21] Shigaki S, Fikri M R, Hernandez Reyes C, Sakurai T, Ando N, Kurabayashi D, Kanzaki R and Sezutsu H 2018 Animal-in-the-loop system to investigate adaptive behavior *Adv. Robot.* **32** 945–53

[22] Lan B, Kanzaki R and Ando N 2019 Dropping counter: a detection algorithm for identifying odour-evoked responses from noisy electroantennograms measured by a flying robot *Sensors* **19** 4574

[23] Anderson M J, Sullivan J G, Brink K, Talley J, Fuller S and Daniel T 2019 The Smellicopter, a bio-hybrid odor localizing nano air vehicle *2019 IEEE/RSJ Int. Conf. on Intelligent Robot. Sys. (IROS)* pp 6077–82

[24] Fandino R A *et al* 2019 Mutagenesis of odorant coreceptor Orco fully disrupts foraging but not oviposition behaviors in the hawkmoth *M. sexta Proc. Natl Acad. Sci. USA* **116** 15677–85

[25] Fuller S B, Straw A D, Peek M Y, Murray R M and Dickinson M H 2014 Flying Drosophilastabilize their vision-based velocity controller by sensing wind with their antennae *Proc. Natl Acad. Sci. USA* **111** E1182–91

[26] Sane S P, Dieudonné A, Willis M A and Daniel T L 2007 Antennal mechanosensors mediate flight control in moths *Science* **315** 863–6

[27] Willis M A, Ford E A and Avondet J L 2013 Odor tracking flight of male *M. sexta* moths along plumes of different cross-sectional area *J. Comp. Physiol.* A **199** 1015–36

[28] Lee J K and Strausfeld N J 1990 Structure, distribution and number of surface sensilla and their receptor cells on the olfactory appendage of the male moth *M. sexta J. Neurocytol.* **19** 519–38

[29] Sane S P and Jacobson N P 2005 Induced airflow in flying insects II. Measurement of induced flow *J. Exp. Biol.* **209** 43–56

[30] Reisenman C E, Riffell J A, Duffy K, Pesque A, Mikles D and Goodwin B 2012 Species-specific effects of herbivory on the oviposition behavior of the moth Manduca sexta *J. Chem. Ecol.* **39** 76–89

[31] Voges N, Chaffiol A, Lucas P and Martinez D 2012 Reactive searching and infotaxis in odor source localization *PLoS Comput. Biol.* **10** e1003861

[32] Harvey D J, Lu T F and Keller M 2008 Comparing insect-inspired chemical plume tracking algorithms using a mobile robot *IEEE Trans. Robot.* **24** 307–17

[33] Tsang W M, Stone A L, Otten D, Aldworth Z N, Hidebrand J G, Levine R D and Voldman J 2012 Insect-machine interface: a carbon nanotube-enhanced flexible neural probe *J. Neurosci. Methods* **204** 355–65

[34] Daly D C, Mercier P P, Bhardwaj M, Stone A L, Aldworth Z N, Daniel T L, Voldman J, Hildebrand J G and Chandrakasan A P 2010 A pulsed UWB receiver SoC for insect motion control *IEEE J. Solid-State Circuits* **45** 153–66

[35] Li Y, Wu J and Sato H 2018 Feedback control-based navigation of a flying insect-machine hybrid robot *Soft Robot.* **5** 365–74

[36] Sato H, Berry C W, Peeri Y, Baghoomian E, Casey B E, Lavella G, VandenBrooks J M, Harrison J F and Maharbiz M M 2009 Remote radio control of insect flight *Frontiers Integr. Neurosci.* **3** 24

[37] Ricotti L *et al* 2017 Biohybrid actuators for robotics: a review of devices actuated by living cells *Sci. Robot.* **2** 1–17

[38] Shields V D C and Hildebrand J G 2001 Responses of a population of antennal olfactory receptor cells in the female moth Manduca sext a to plant-associated volatile organic compounds *J. Comp. Physiol.* A **186** 1135–51

[39] Hansson B S, Carlsson M A and Kalinovà B 2003 Olfactory activation patterns in the antennal lobe of the sphinx moth, *M. sexta J. Comp. Physiol.* A **189** 301–8

[40] Fraser A M, Mechaber W L and Hildebrand J G 2003 Electroantennographic and behavioral responses of the sphinx moth Manduca sexta to host plant headspace volatiles *J. Chem. Ecol.* **29** 1813–33